OFFICE OF NAVAL RESEARCH

GRANT: N00014-93-0545

R & T CODE: 413V005

Technical report # 3

TWO-DIMENSIONAL CONDENSATION OF METHYLGUANIDINIUM NITRATE AT THE WATER/MERCURY INTERFACE

by

T. Wandlowski, G. B. Jameson and R. de Levie

prepared for publication in the
Journal of Electroanalytical Chemistry

Chemistry Department, Georgetown
University, Washington DC 20057

June 26, 1995

REPORT DOCUMENTATION PAGE

Form Approved
OMB No. 0704-0188

1. AGENCY USE ONLY (*Leave blank*)	2. REPORT DATE	3. REPORT TYPE AND DATES COVERED
	June 26, 1995	Technical

4. TITLE AND SUBTITLE

TWO-DIMENSIONAL CONDENSATION OF METHYLGUANIDINIUM NITRATE AT THE WATER/MERCURY INTERFACE

5. FUNDING NUMBERS

N00014-93-1-0545

6. AUTHOR(S)

T. Wandlowski, G. B. Jameson and R. de Levie

7. PERFORMING ORGANIZATION NAME(S) AND ADDRESS(ES)

Chemistry Department, Georgetown University, Washington DC

8. PERFORMING ORGANIZATION REPORT NUMBER

Technical report #3

9. SPONSORING/MONITORING AGENCY NAME(S) AND ADDRESS(ES)

Office of Naval Research, Dept. of the Navy, Arlington VA 22217

10. SPONSORING/MONITORING AGENCY REPORT NUMBER

11. SUPPLEMENTAL NOTES

12a. DISTRIBUTION AVAILABILITY STATEMENT

Approved for public release; distribution unlimited

12b. DISTRIBUTION CODE

13. ABSTRACT (*Maximum 200 words*)

Methylguanidinium nitrate can form a condensed interfacial monolayer, similar to that observed with guanidinium nitrate. However, the presence of the methyl group dramatically changes the effect of the salt monolayer on electrode kinetics

14. SUBJECT TERMS

Two-dimensional condensation
Methylguanidinium nitrate

15. NUMBER OF PAGES

26

16. PRICE CODE

17. SECURITY CLASSIFICATION OF REPORT	18. SECURITY CLASSIFICATION OF THIS PAGE	18. SECURITY CLASSIFICATION OF ABSTRACT	20. LIMITATION OF ABSTRACT
Unclassified	**Unclassified**	**Unclassified**	**Unlimited**

TWO-DIMENSIONAL CONDENSATION OF METHYLGUANIDINIUM NITRATE AT THE MERCURY-WATER INTERFACE

Thomas Wandlowski, Geoffrey B. Jameson and Robert de Levie
Department of Chemistry, Georgetown University, Washington DC 20057 USA

Abstract

Methylguanidinium nitrate can form a condensed interfacial monolayer, similar to that observed with guanidinium nitrate. However, the presence of the methyl group dramatically changes the effect of the salt monolayer on electrode kinetics.

Introduction.

While the properties of compact monolayer films made by two-dimensional condensation of molecules adsorbed at the mercury-water interface have been studied extensively during the past decade, and have been reviewed several times [1-4], considerably less information is available on the formation and electrochemical behavior of compact salt monolayers. Frumkin, Damaskin and Nikolaeva-Fedorovich showed that adsorbed tetrabutylammonium iodide undergoes a two-dimensional change of state [5-8]. In a recent series of papers we reported on the kinetic properties of the compact films formed by tetrabutylammonium cations and a variety of anions [9-11]. Interfacial condensation has also been reported for phenyl-substituted quaternary phosphonium ions in aqueous solutions containing chloride or bromide ions [12-18], and for several carboxylates, sulfonates and sulfates [19,20].

Among the cations that can form compact monolayer films at the mercury-water interface, the behavior of the planar guanidinium cation is interesting because it is very specific about the nature of the anion, and forms such films only with nitrate (and, to some extent, with sulfate). Electrochemical [21,22] and crystallographic [22] results suggest that the interfacial organization of guanidinium nitrate is most likely a planar, pseudo-hexagonal array, in which each guanidinium and nitrate ion is held in place by six hydrogen bonds to its neighboring counterions. The resulting lace-like structure contains fairly large holes, despite the fact that all hydrogen-bonding valencies of the ions are saturated. The holes

are large enough to accommodate a water molecule. This may explain why we have so far not found any inhibitory effect of compact guanidinium nitrate films on the kinetics of "simple" electrode reactions, such as the polarographic reductions of Cd(II), Tl(I), $Co(NH_3)_6^{3+}$, $S_2O_8^{2-}$ and $Cr_2O_7^{2-}$.

In the present communication we will report on the interfacial behavior of the monomethyl derivative methylguanidinium nitrate, which also forms compact salt monolayers at the mercury-water interface. Our electrochemical studies of the kinetics of the formation of such films, of its stability, and of its effect on faradaic processes, will be supplemented by an X-ray redetermination of the three-dimensional crystal. Comparison with the earlier-reported behavior of guanidinium nitrate clearly establishes the crucial role of the methyl group.

Experimental methods.

All capacitance measurements were made on a hanging mercury electrode of 2.37_5 mm^2 area, formed at the end of an unsiliconized glass capillary in a PAR 303 mercury dispenser. The auxiliary electrode was a platinum wire, and an external saturated calomel electrode, connected through a double liquid junction, and maintained at room temperature, was the reference electrode. All potentials given are referred to this electrode. The cell temperature was controlled to within $\pm 0.2^{o}C$ and, unless otherwise stated, was maintained at $+5^{o}C$.

The capacitance was measured by superimposing a 1.59 KHz sinewave of 2.5 mV amplitude on a voltage step or voltage ramp. Maximum iR compensation short of oscillations was used to minimize the uncompensated solution resistance. The cell current was converted into a voltage, and its ac component amplified, synchronously rectified with a lock-in amplifier, digitized, and stored in an AT-type computer for subsequent data processing.

The polarographic measurements were made with an IBM EC 225 using a dropping mercury electrode with a mercury flow rate of 0.6 mg s^{-1} and a drop time of 15.2 s at open circuit.

All solutions were prepared from pyrodistilled water and Merck Suprapur or Sigma chemicals. The supporting electrolyte solutions were treated with activated charcoal before use. Methylguanidinium nitrate was obtained by quantitative precipitation of methylguanidinium chloride (Sigma M 0377) with silver nitrate.

Crystals of methylguanidinium nitrate were grown in a saturated aqueous solution of the salt, kept for several weeks in a refrigerator at a temperature just above $0^{o}C$. A good harvest of crystals was obtained.

The capacitance as a function of potential, concentration and temperature.

Figures 1 and 2 illustrate the differential capacitance of methylguanidinium nitrate at the interface between mercury and water or aqueous 0.5 M nitrate, respectively. These measurements show wide capacitance pits with pronounced hysteresis. Comparison of these curves with those reported earlier for guanidinium nitrate [21,22] shows them to be shifted to more positive potentials; only at above-ambient temperatures is the positive pit edge observable within the range of ideal polarization of the mercury-solution interface. These compact films show a remarkable stability to temperature, being still observable at 60°C, see Fig. 3. Unfortunately, the inaccessibility of the positive pit edge at ambient and below-ambient temperatures made impractical a quantitative study of the pit width as a function of methylguanidinium and nitrate ions along the lines of that reported for guanidinium nitrate [22].

Figs. 1-3

Comparison with crystallographic data.

We redetermined the crystal structure of methylguanidinium nitrate originally reported by Curtiss and Pasternak [23]. Details about the crystal and the data collection method used can be found in Table 1. The resulting atomic coordinates are listed in Table 2, while Table 3 shows the corresponding bond angles and bond distances. The general features of their crystal structure are confirmed, but with features such as the hydrogen bonding network precisely revealed. The crystal exhibits a layered structure. Within the layers, methylguanidinium and nitrate ions alternate. Each cation has two anions as its nearest neighbors, and one anion at a slightly larger distance; likewise, each anion has two nearest-neighboring cations and one a little further away.

Each nitrate ion has five hydrogen bonds to the neighboring methylguanidinium ions (two each to its two closest neighbors), and each methylguanidinium ion has five hydrogen bonds (again two each to its two closest neighbors) linking it to the three neighboring nitrate ions. The N-H···O hydrogen bonds exhibit bond angles between 167° and 177°, close to the ideal value of 180°. The pair of N-O···H angles at the two oxygens each carrying two hydrogen bonds are about 112° and 130°, compared to the ideal value of 120°. All hydrogen bonds lie in the plane through the methylguanidinium and nitrate ions. The resulting planar structure (except for the two methyl hydrogens located symmetrically above and below the plane) is shown in Fig. 4a. The crystal structure exhibits no disorder.

The area per methylguanidinium nitrate ion pair in the plane is 0.482_2 nm^2, barely larger than that for guanidinium nitrate (0.477 nm^2) because the methyl group mostly fills up the hole in the guanidinium nitrate structure [22].

Tables 1-4

Fig. 4

Comparison with the packing in guanidinium nitrate shows the consequences of replacing one hydrogen on the guanidinium ion by a methyl group: only five hydrogen bonds are now possible, and the presence of the methyl group forces the N-O H bond angles away from 120^o. The resulting arrangement of the ions in the plane can best be described as that of linear chains or ribbons of alternating anions and cations, parallel to the crystallographic c axis, held together by double hydrogen bonds between adjacent nearest-neighbor ions, see Fig. 4b. Between adjacent ribbons there is only one hydrogen bond per cation-anion pair, although the possibility of a weak addition hydrogen bond to one of the methyl hydrogens cannot quite be excluded (C2 O2 323.7 pm, H6 O2 249 pm, C-H O2 137^o but N1-O2 H 169^o). In this way, all five nitrogen-bonded hydrogens in the methylguanidinium cation are hydrogen-bonded to adjacent nitrate oxygens.

The atomic distances between the planes do not indicate any specific interactions. The layers pack so that anions find themselves surrounded by cations, and vice versa, thus maximizing their Coulombic interactions. The closest interplanar contact between atoms is between the methylated nitrogen atom and the nitrate nitrogen atom at 325 pm and a nitrogen oxygen atom at 331 pm, compared to the interplanar separation of b/2 = 321 pm.

It is the layer structure of the three-dimensional crystal, with only Coulomb interaction between adjacent layers but strong hydrogen bonding within each layer, which suggests that the molecular organization in the compact monolayer at the mercury-solution interface may well resemble that in the individual layers in the crystal. In this scenario, the interfacial condensation is then caused by the loss of water of hydration as the ions hydrogen-bond to counterions rather than to water molecules, just as they would when growing a three-dimensional crystal from a saturated aqueous solution. We have recently discussed several other instances where the structure of three-dimensional crystals exhibiting layered structures may be relevant to the interfacial organization of compact monolayer films [24].

The kinetics of film formation.

Kinetic studies are hampered by the fact that we cannot establish satisfactory initial conditions for simple transient experiments, because there are no potentials at which neither methylguanidinium nor nitrate is adsorbed. In the present study we have mostly used -1.4 V as our point of departure for potential step measurements. Figures 5 and 6 illustrate two sets of capacitance transients obtained by jumping into the region of the negative pit edge. Steps into the center of the pit show transients which resemble single exponentials (Fig. 5) although their Avrami analysis reveals that this applies only to their initial parts. As the final potential approaches the pit edge, the transients acquire a more pronounced sigmoid shape usually associated with film formation, see Fig. 6. Nonetheless, the Avrami plots are clearly non-linear, and suggest the presence of two successive processes, or perhaps a switch from one rate-determining process to another as time proceeds. Double potential step experiments, as illustrated in Fig. 7, yield similar results.

Figs. 5-7

By forcing the nucleation to be "instantaneous", the double potential step allows us to study the time-dependence of the kinetics of growth. The traditional method of doing so is based on the Avrami plot, in which we display $\ln \Theta_x$ versus $\ln(t)$, where t is time and the extended area fraction Θ_x is given by the Canac equation [25]

$$\Theta = 1 - \exp[-\Theta_x] \qquad (1)$$

In equation (1), the area fraction Θ covered by the compact film can be expressed in terms of the measured interfacial capacitance C and its initial and final values, C_0 and C_∞ respectively, as

$$\Theta = (C_0 - C)/(C_0 - C_\infty) \qquad (2)$$

Combining eqns. (1) and (2) yields

$$\Theta_x = \ln[1-\Theta]^{-1} = \ln[(C_0-C_\infty)/(C-C_\infty)] \qquad (3)$$

which shows how Θ_x can be expressed directly in terms of the experimentally accessible capacitances C_0, C and C_∞.

In a double potential step experiment such as shown in Fig. 7, the number of nuclei N is constant after the transition $E_1 \rightarrow E_2$, and all clusters are of approximately the same age and, therefore, presumably of the same area a, so that Θ_x is

$$\Theta_x = N\,a\,/\,A \qquad (4)$$

where A is the total exposed interfacial area. Clearly, the slope $d \ln \Theta_x / d \ln t$ in the Avrami plot has the value of $d \ln a / d \ln t$.

As long as a follows a simple power law in time, such as $a = kt^m$, the Avrami plot will exhibit a simple slope m. A value m = 1 may reflect inherently slow unidirectional growth (as in the growth of strands and fibers) or growth limited by two-dimensional diffusion. A slope m = 2 may correspond to slow two-dimensional growth. The data shown in the inset of Fig. 7 suggest a transition from m = 1 to m = 2 during the transient.

An alternative method to analyze these data can be based on a method suggested by Deutscher & Fletcher [26]. Their approach, as applied here to non-faradaic capacitance measurements, is equivalent to examining the derivative of eqn. (4), i.e., to plotting

$$\frac{d\,\Theta_x}{d\,t} = \frac{1}{(1-\Theta)\,(C_0 - C_\infty)}\,\frac{dC}{dt} = \frac{N}{A}\,\frac{da}{dt} \qquad (5)$$

For $a = kt^m$, eqn.(5) yields $d\,\Theta_x / d\,t = (Nmk/A)\,t^{m-1}$, which is constant for m = 1 and linear in t for m = 2. Fig. 8 shows an analysis of curve 2 in Fig. 7 according to eqn. (5). Such an analysis supports the same conclusion as reached on the basis of the Avrami plot, namely that the growth rate varies with time and, more specifically, appears to switch from m = 1 to $m \approx 2$ during the transient, as the coverage approaches 50%. However, as in all differentiation of experimental data, this method is strongly affected by experimental "noise", and therefore yields a much less reliable experimental criterion than the Avrami plot.

Fig. 8

In view of the crystal structure discussed earlier, one can envision a process in which growth first leads to the formation of doubly hydrogen-bonded ribbons, which subsequently align to form a two-dimensional film. While such a sequence of events is kinetically and energetically plausible, and might explain the observed kinetic behavior, we have no *direct* evidence to support it, so that it must remain a hypothesis.

Effect on Faradaic reactions

In contrast to the situation observed with guanidinium nitrate, films formed with methylguanidinium nitrate strongly inhibit the polarographic reduction of O_2 , $S_2O_8^{2-}$, $Co(NH_3)_6^{3+}$ and Cu^{2+}. For the first three of these, in which the reduction product remains in solution, so that the integrity of the film need not be breached, the inhibition is independent of adsorbate concentration as long as the latter is sufficient to maintain a compact film. Figure 9 illustrates this behavior for the polarographic reduction of hexamminecobaltate.

Fig. 9

The polarographic reduction of cupric ions is shown in Fig. 10. In this case, the strong inhibition depends on the concentration of the methylguanidinium nitrate, as one would expect for a process in which the film must be opened in order to let the copper pass to the mercury phase [27,28].

Fig. 10

Discussion.

The most interesting aspects of this study are the unusual kinetics of film formation, and the contrast between the inhibition behaviors of the compact films of guanidinium nitrate and methylguanidinium nitrate. We have already commented on the difference in the growth kinetics, and given a tentative explanation for the observed behavior. We will now indicate in what direction we look for an interpretation of the qualitative difference in the inhibition behavior. We start with the observation that methylguanidinium films inhibit the same faradaic processes that guanidinium nitrate films apparently let pass unhindered. Since both films are made from salts, their ionic nature doesn't explain the observed difference. However, the assumed molecular orientation, based on the structure of the corresponding three-dimensional layered crystals, seems to furnish a reasonable interpretation. We already noted that the proposed structure of the guanidinium nitrate film has large holes, each of which can possibly accommodate a water molecule. The presence of this hole may facilitate charge transfer. Again judging from its crystal structure, the methyl groups in methylguanidinium nitrate approximately occupy the positions of the holes in the corresponding structure of guanidinium nitrate. We surmise that this is a likely reason why compact methylguanidinium films are strongly inhibiting the very same Faradaic processes which guanidinium nitrate leaves alone.

The only piece of the puzzle which has not yet fallen into place is the strong shift of the center of the pit region towards positive potentials upon introduction of the methyl group.

Acknowledgement

Support from ONR through grant N-00014-93-1-0545 is gratefully acknowledged. The single-crystal X-ray diffractometer used was purchased with financial aid from NSF grant CHE-9115394.

References

1. R. de Levie, Advances in electrochemistry and electrochemical engineering, H. Gerischer, ed., Wiley, New York, *13* (1985) 1.
2. C. Buess-Herman, Trends in interfacial electrochemistry, A. F. Silva, ed., Reidel, Dordrecht, 1986, p. 205.
3. R. de Levie, Chem. Revs., *88* (1988) 599.
4. C. Buess-Herman, Adsorption of molecules at metal electrodes, J. Lipkowski and P. N. Ross, eds, VCH, New York, 1992, p. 77.
5. A. N. Frumkin, B. B. Damaskin and N. V. Nikolaeva-Fedorovich, Dokl. Akad. Nauk SSSR, *115* (1957) 751.
6. A. N. Frumkin and B. B. Damaskin, Dokl. Akad. Nauk SSSR, *129* (1959) 862.
7. B. B. Damaskin and N. V. Nikolaeva-Fedorovich, Zh. Fiz. Khim., *35* (1961) 1279.
8. A. N. Frumkin, Trans. Symp. Electrode Processes, E. Yeager ed., Wiley, New York, 1961, p. 1.
9. T. Wandlowski and R. de Levie, J. Electroanal. Chem., *329* (1992) 103.
10. T. Wandlowski and R. de Levie, J. Electroanal. Chem., *345* (1993) 413.
11. T. Wandlowski and R. de Levie, J. Electroanal. Chem., *352* (1993) 279.
12. Y. V. Michailik and B. B. Damaskin, Elektrokhimiya, *15* (1979) 478.
13. H. D. Dörfler and E. Müller, J. Electroanal. Chem., *105* (1979) 383.
14. E. Müller, H. Matschiner and H. D. Dörfler, Z. Phys. Chem., *260* (1979) 804.
15. H. D. Dörfler and E. Müller, J. Electroanal. Chem., *121* (1981) 153.
16. M. H. Saffarian and R. de Levie, J. Electroanal. Chem., *189* (1985) 325.
17. R. Sridharan, M. H. Saffarian and R. de Levie, J. Electroanal. Chem., *236* (1987) 371.
18. A. Anastopoulos and A. Christodoulou, Coll. Czech. Chem. Comm., *53* (1988) 732.
19. B. B. Damaskin, N. V. Nikolaeva-Fedorovich and R. W. Ivanova, Zh. Fiz. Khim., *34* (1960) 894.
20. H. Jehring, Elektrosorptionsanalyse mit Wechselstrompolarographie, Academie-Verlag, Berlin (1974).
21. S. L. Dyatkina, B. B. Damaskin and M. Z. Vygotskaya, Elektrokhimiya, *16* (1980) 996.
22. T. Wandlowski, G. Jameson and R. de Levie, J. Phys. Chem., *97* (1993) 10119.
23. R. M. Curtiss and R. A. Pasternak, Acta Cryst. *8* (1955) 675.
24. R. de Levie and T. Wandlowski, J. Electroanal. Chem., (JEC 02932).
25. F. Canac, Compt. Rend., *196* (1933) 51.
26. R. L. Deutscher and S. Fletcher, J. Electroanal. Chem., *153* (1983) 67.
27. R. Srinivasan and R. de Levie, J. Electroanal. Chem., *201* (1986) 145.
28. J. Lipkowski, C. Buess-Herman, J. P. Lambert & L. Gierst, J. Electroanal. Chem., *202* (1986) 169.

Figure legends.

Fig. 1. The interfacial capacitance C of mercury in contact with aqueous solutions of methylguanidinium nitrate as a function of the applied potential E vs. SCE. Guanidinium nitrate concentrations: (1) 0.05 M; (2) 0.075 M; (3) 0.10 M; (4) 0.25 M. Temperature 5°C, measuring frequency 1.59 KHz, amplitude 2.5 mV, voltage scan rate -5 mV s^{-1}. Reverse scans, with a scan rate of +5 mV s^{-1}, are sketched in with a thin broken line and identified as (1′), (2′), etc. Note the unusually large hysteresis loops.

Fig. 2. The same as in Fig. 1, except that the measurements were made at a constant nitrate concentration of 0.5 M, with aqueous solutions containing x M of guanidinium nitrate + (0.5-x) M of sodium nitrate, where x is (1) 0 M; (2) 0.0015 M; (3) 0.0045 M; (4) 0.013 M; (5) 0.05 M. Again, reversed scans are shown as thin broken lines.

Fig. 3. The temperature dependence of the interfacial capacitance of mercury in contact with an aqueous solution containing 0.05 M methylguanidinium nitrate and 0.45 M sodium nitrate. The potential scan started 10 s after drop formation at -0.200 V. Temperatures: (1) 31°C; (2) 40°C; (3) 50°C; (4) 55°C; (5) 61°C; (6) 65°C; (7) 66°C. All other conditions are as in Fig. 1.

Fig. 4. (a) The arrangement of the methylguanidinium and nitrate ions in the (020) crystal plane, shown as a space-filling model, using van der Waals radii of 0.127, 0.082, 0.116 and 0.120 nm for C, H, O and N respectively. (b) The same overlaid with a stick diagram showing the covalent bonds (solid lines) and the hydrogen bonds (broken lines) between ions in a ribbon and between adjacent ribbons (dotted lines). One ribbon is emphasized by shading.

Fig. 5. Capacitance transients following single potential steps from E_0 = -1.400 V to the following final potentials E_1: (1) -0.690 V; (2) -0.700 V; (3) -0.710 V; (4) -0.720 V; (5) -0.730 V; (6) -0.740 V. Solution: 0.477 M $NaNO_3$ + 0.023 M methylguanidinium nitrate, temperature 5°C. The inset shows the corresponding Avrami plots.

Fig. 6. Capacitance transients as in Fig. 5, but with the following final potentials E_1: (1) -0.765 V; (2) -0.770 V; (3) -0.775 V; (4) -0.777_5 V; (5) -0.780 V; (6) -0.782_5 V. Solution: 0.477 M $NaNO_3$ + 0.023 M methylguanidinium nitrate, temperature 5°C. The inset shows the corresponding Avrami plots.

Fig. 7. Capacitance transients following the application of a double potential step from E_0 = -1.400 V, τ_0 = 10 s to E_1 = -0.770 V for τ_1 s to the final potential E_2 = -0.810 V. Nucleation times τ_1 at E_1 = -0.770 V: (1) 0 s; (2) 0.25 s. The transients shown are recorded following the transition $E_0 \rightarrow E_1$. Curve (3) shows the transient following a single step from E_0 = -1.400 V, τ_0 = 10 s to E_1 = -0.770 V. Solution: 0.477 M $NaNO_3$ + 0.023 M methylguanidinium nitrate, temperature 5^oC. The inset shows the Avrami plots for curves 2 and 3.

Fig. 8. The growth transient of Fig. 7 curve 2 analyzed according to equation (5). The capacitance C(t) was differentiated with a moving quadratic encompassing m contiguous equidistant data points, using the Savitzky-Golay method [29]. The same method was also used to smooth the factor $1/(1-\Theta)$, again with an m-th order polynomial, whereupon the two were multiplied and, finally, scaled by the factor $1/(C_o-C_\infty)$. The two curves shown are for m = 11 (line) and m = 25 (individual points); the latter is the longest data string for which coefficients are listed by Savitzky and Golay [29]. The same 12-second stretch of the transient was analyzed as is shown in curve 2 of Fig. 7.

Fig. 9. Polarograms of aqueous x M methylguanidinium nitrate (MGN) + (0.5 - x) M $NaNO_3$ + 0.25 mM $[Co(NH_3)_6]_2[SO_4]_3$ where (1): x = 0 and (2): x = 0.1 M. The polarograms for 0.001 M ≤ [MGN] ≤ 0.5 M are similar except for the potential at which the compact MGN film dissolves, as indicated for the 0.1 M solution by an arrow. Temperature 5.0^oC, drop time 15.2 s, mercury flow rate 0.6 mg s^{-1} and voltage scan rate -1 mV s^{-1}.

Fig. 10. Polarogram of an aqueous solution of x M MGN + (0.5 - x) M $NaNO_3$ + 0.5 mM $Cu(NO_3)_2$, where x has the following values: (1) 0; (2) 0.0125 M; (3) 0.025 M; (4) 0.05 M; (5) 0.10 M; (6) 0.20 M. Broken lines indicate lower precision due to polarographic maxima early in drop life. All other conditions as in Fig. 9.

Tables.

Crystal data:

Empirical formula	$C_2 H_8 N_4 O_3$
Color & habit	clear, colorless block
Dimensions	0.4 mm x 0.4 mm x 0.5 mm
Crystal system	orthorhombic
Space group	Pnma
Unit cell dimensions	a = 1323.8 ± 0.1 pm
	b = 642.9 ± 0.1 pm
	c = 728.5 ± 0.1 pm
Unit cell volume	0.6200 ± 0.0001 nm^2
Z (number of molecules per unit cell)	4
Calculated density	1.458 Mg m^{-3}
Absorption coefficient	0.132 mm^{-1}
F(000) (total number of electrons per unit cell)	288

Data collection:

Diffractometer used	Siemens P4/RA
Power used	14.4 kW
Temperature	295°K
Radiation	Mo K_α, λ = 71.073 pm
Monochromator	Highly oriented graphite crystal
2Θ range	7.0° to 45°
Scan type	ω
Scan speed	variable, 2 to 30° min^{-1} in ω
Scan range	0.46°
Background measurement	stationary crystal and stationary counter at beginning and end of scan, each for 50% of total scan time
Standard reflections	3 measured for every 100 reflections
Index ranges	$-1 \le h \le 18$
	$-1 \le k \le 9$
	$-1 \le l \le 10$
Reflections collected	1350
Independent reflections	963 (R_{int} = 1.07%)
Observed reflections	708 ($F > 4.0\,\sigma(F)$)
Absorption correction	none applied

Structure analysis and refinement:

System used	Siemens SHELXTL PLUS PC version
Solution method	Direct methods
Refinement method	Full-matrix least-squares
Quantity minimized	$\Sigma w(F_o-F_c)^2$
Analysis for hydrogen atoms	Refined isotropically
Weighting scheme	$w^{-1} = \sigma^2(F) + 0.0008\ F^2$
Number of parameters refined	78
Final R indices (observed data)	R = 4.06%, wR = 4.81%
R indices (all data)	R = 5.25%, wR = 6.29%
Goodness-of-fit	1.39
Largest and mean Δ/σ	0.295, 0.044
Data-to-parameter ratio	9.1 : 1
Largest difference peak	0.21 eÅ^{-3}
Largest difference hole	-0.19 eÅ^{-3}

Table 1. Summary of the specifics of the crystal data, the data collection method, and the structure analysis and refinement used.

	x	y	z	U_{eq}
methylguanidinium:				
C(1)	+0.07502 ±0.00013	+0.2500	+0.85834 ±0.00021	+0.00310 ±0.00005
C(2)	+0.21902 ±0.00016	+0.2500	+0.64761 ±0.00029	+0.00464 ±0.00007
N(2)	+0.13420 ±0.00013	+0.2500	+1.00421 ±0.00020	+0.00386 ±0.00005
N(3)	−0.02486 ±0.00013	+0.2500	+0.87800 ±0.00023	+0.00458 ±0.00006
N(4)	+0.11234 ±0.00011	+0.2500	+0.69004 ±0.00020	+0.00364 ±0.00005
H(1)	+0.1982 ±0.0025	+0.2500	+1.0028 ±0.0036	+0.0057 ±0.0008
H(2)	+0.0988 ±0.0021	+0.2500	+1.1155 ±0.0034	+0.0045 ±0.0007
H(3)	−0.0531 ±0.0020	+0.2500	+0.9814 ±0.0037	+0.0059 ±0.0008
H(4)	−0.0626 ±0.0022	+0.2500	+0.7715 ±0.0037	+0.0057 ±0.0007
H(5)	+0.0686 ±0.0020	+0.2500	+0.5942 ±0.0033	+0.0047 ±0.0007
H(6)	+0.2214 ±0.0025	+0.2500	+0.5193 ±0.0049	+0.0091 ±0.0012
H(7)	+0.2491 ±0.0012	+0.3707 ±0.0033	+0.6978 ±0.0028	+0.0076 ±0.0006
H(8)	+0.2491 ±0.0012	+0.1293 ±0.0033	+0.6978 ±0.0028	+0.0076 ±0.0006
nitrate:				
N(1)	−0.09185 ±0.00012	+0.2500	+0.36090 ±0.00019	+0.00362 ±0.00005
O(1)	−0.13255 ±0.00011	+0.2500	+0.51486 ±0.00019	+0.00553 ±0.00006
O(2)	−0.14484 ±0.00011	+0.2500	+0.22144 ±0.00020	+0.00507 ±0.00005
O(3)	+0.00214 ±0.00010	+0.2500	+0.34813 ±0.00020	+0.00528 ±0.00006

Table 2. Fractional atomic coordinates x, y,and z, and equivalent isotropic displacement coefficients U_{eq} (defined as one-third of the trace of the orthogonalized U_{ij} tensor). Atomic coordinates in nm can be obtained from the fractional coordinates x, y and z through multiplication by the unit cell dimensions a = 1.3238 nm, b = 0.6429 nm and c = 0.7285 nm respectively.

See Fig. 4a for the numbering used to identify the various atoms.

methylguanidinium:

C(1) - N(2)	132.0 ± 0.2	N(2) - H(1)	85 ± 3
C(1) - N(3)	133.0 ± 0.2	N(2) - H(2)	94 ± 3
C(1) - N(4)	132.2 ± 0.2	N(3) - H(3)	84 ± 3
N(4) - C(2)	144.6 ± 0.3	N(3) - H(4)	92 ± 3
		N(4) - H(5)	91 ± 3
		C(2) - H(6)	94 ± 4
		C(2) - H(7)	95 ± 2
		C(2) - H(8)	95 ± 2

nitrate:

N(1) - O(1)	124.4 ± 0.2
N(1) - O(2)	123.5 ± 0.2
N(1) - O(3)	124.8 ± 0.2

interionic nitrogen-oxygen distances involving hydrogen bonds and the corresponding hydrogen-oxygen distances:

N(3) ··· O(1)	300.5 ± 0.2	H(4) ··· O(1)	209 ± 3
N(4) ··· O(3)	288.7 ± 0.2	H(5) ··· O(3)	204 ± 3
N(2) ··· O′(3)	305.5 ± 0.2	H(2) ··· O′(3)	212 ± 3
N(3) ··· O′(2)	296.1 ± 0.2	H(3) ··· O′(2)	213 ± 3
N″(2) ··· O(1)	309.1 ± 0.2	H″(1) ··· O(1)	224 ± 3

Table 3. Bond lengths, in pm. See Fig. 4a for the numbering used to identify the various atoms.

methylguanidinium:

N(2) - C(1) - N(3)	120.2 ± 0.2
N(3) - C(1) - N(4)	118.1 ± 0.2
N(4) - C(1) - N(2)	121.7 ± 0.2
C(1) - N(4) - C(2)	124.3 ± 0.2
C(1) - N(2) - H(1)	126 ± 2
H(1) - N(2) - H(2)	121 ± 2
H(2) - N(2) - C(1)	114 ± 2
C(1) - N(3) - H(3)	123 ± 2
H(3) - N(3) - H(4)	121 ± 3
H(4) - N(3) - C(1)	117 ± 2
C(1) - N(4) - H(5)	118 ± 2
H(5) - N(4) - C(2)	117 ± 2
N(4) - C(2) - H(6)	104 ± 2
N(4) - C(2) - H(7)	109 ± 1
H(6) - C(2) - H(7)	112 ± 2
H(7) - C(2) - H(8)	110 ± 2
H(7) - C(2) - N(4)	109 ± 1

nitrate:

O(1) - N(1) - O(2)	119.7 ± 0.2
O(2) - N(1) - O(3)	120.3 ± 0.1
O(1) - N(1) - O(3)	119.9 ± 0.2

hydrogen bonds:

N(3) - H4 ··· O(1)	174 ± 1
N(4) - H5 ··· O(3)	167 ± 1
N(2) - H2 ··· O′(3)	173 ± 1
N(3) - H3 ··· O′(2)	172 ± 1
N"(2) - H"1 ··· O(1)	177 ± 1

Table 4. Bond angles, in degrees. See Fig. 4a for the numbering used to identify the various atoms.

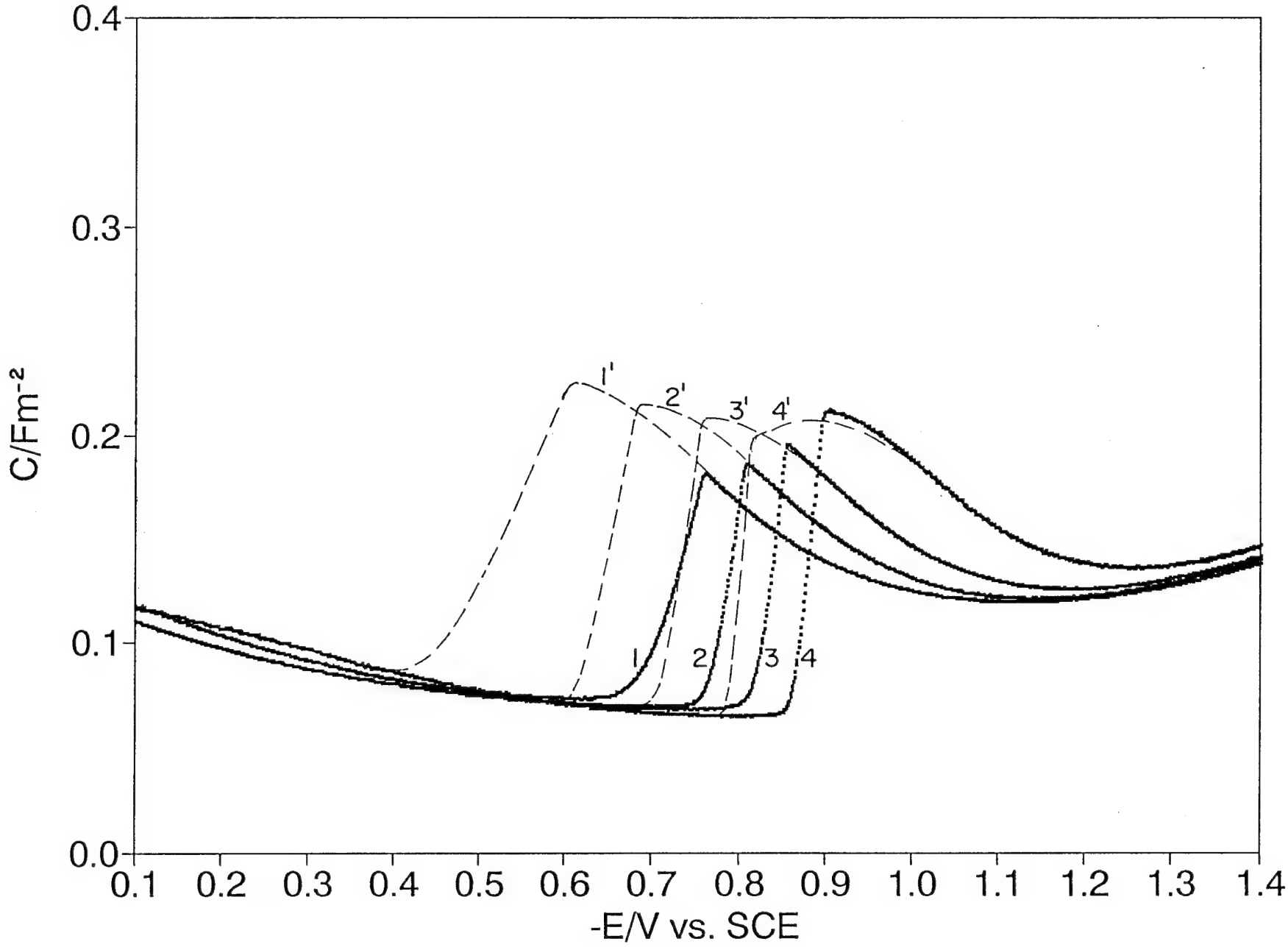
0.4
0.3
0.2
0.1
0.0
C/Fm⁻²
1'
2'
3'
4'
1
2
3
4
0.1 0.2 0.3 0.4 0.5 0.6 0.7 0.8 0.9 1.0 1.1 1.2 1.3 1.4
-E/V vs. SCE

FIG. 1

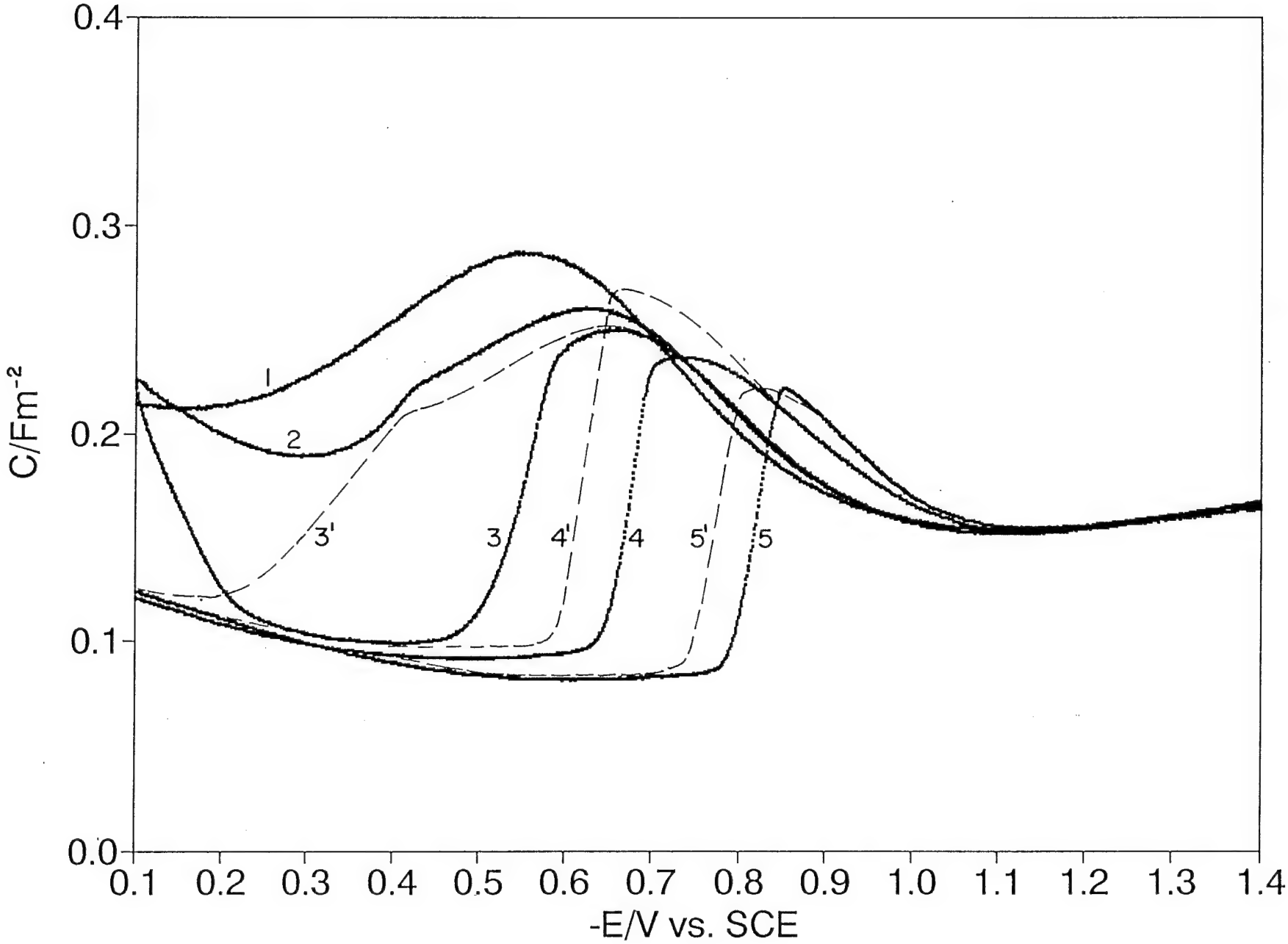
0.4
0.3
0.2
0.1
0.0
C/Fm-2
1
2
3'
3
4'
4
5'
5
0.1 0.2 0.3 0.4 0.5 0.6 0.7 0.8 0.9 1.0 1.1 1.2 1.3 1.4
-E/V vs. SCE

FIG. 2

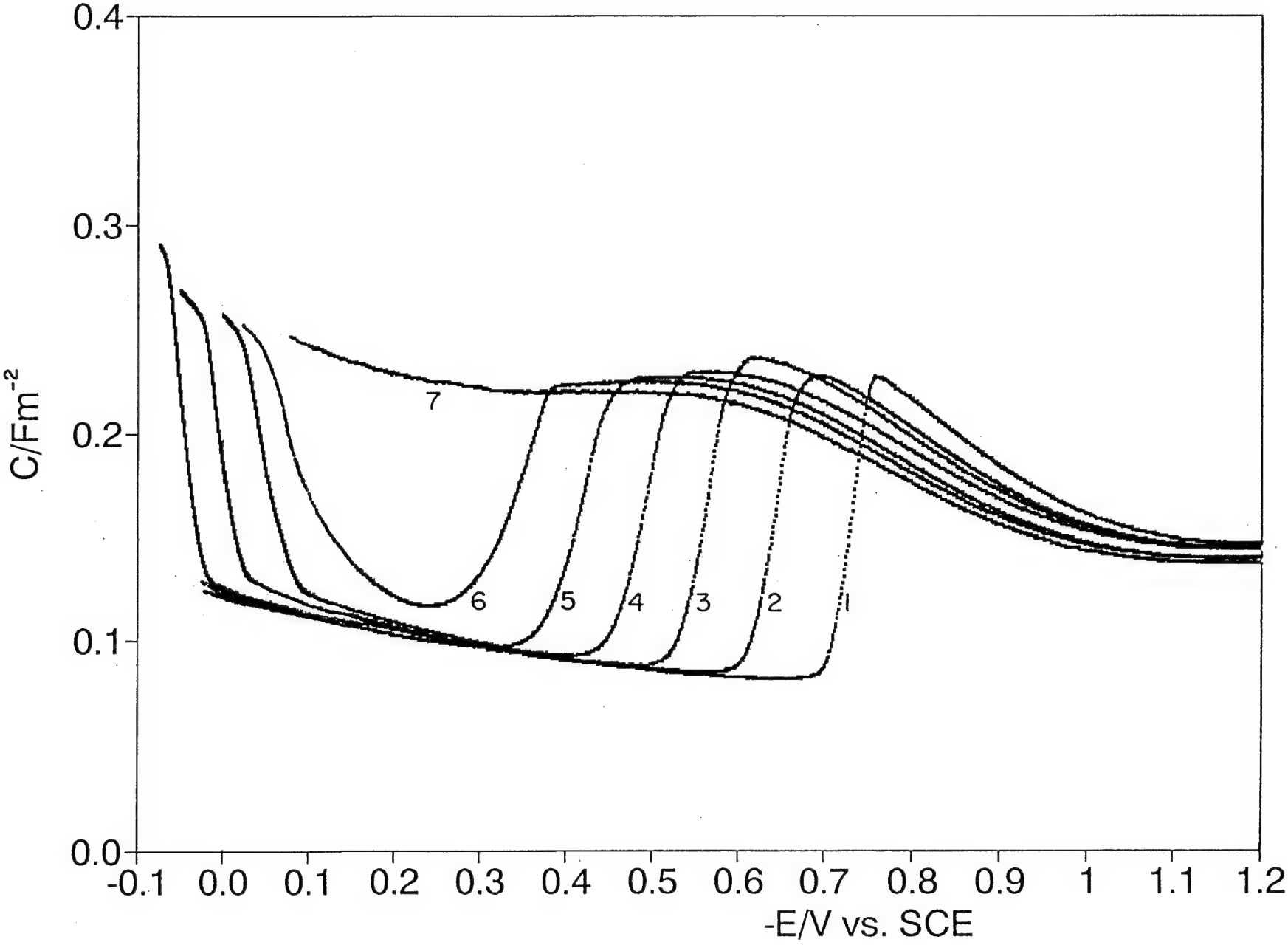
0.4
0.3
0.2
0.1
0.0
C/Fm-2
7
6
5
4
3
2
1
-0.1
0.0
0.1
0.2
0.3
0.4
0.5
0.6
0.7
0.8
0.9
1
1.1
1.2
-E/V vs. SCE

FIG. 3

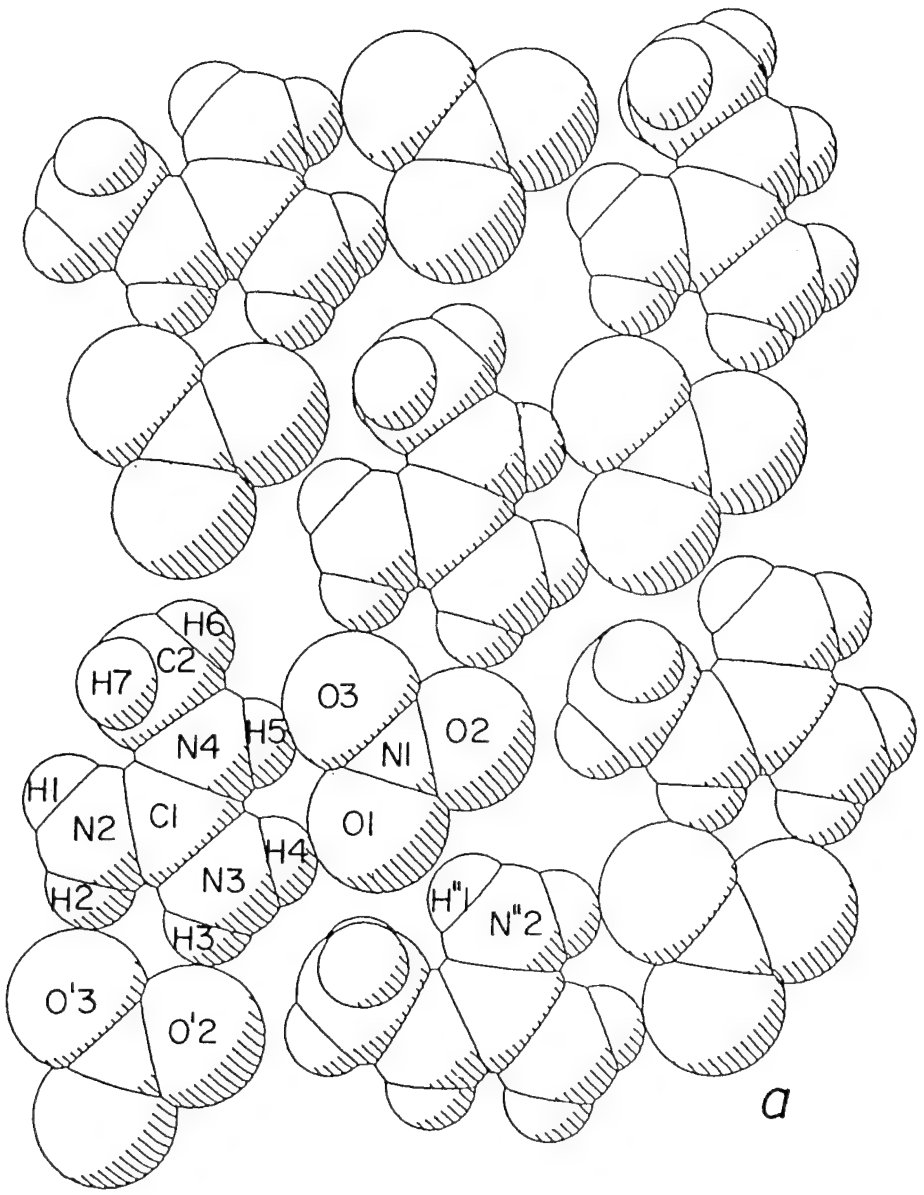

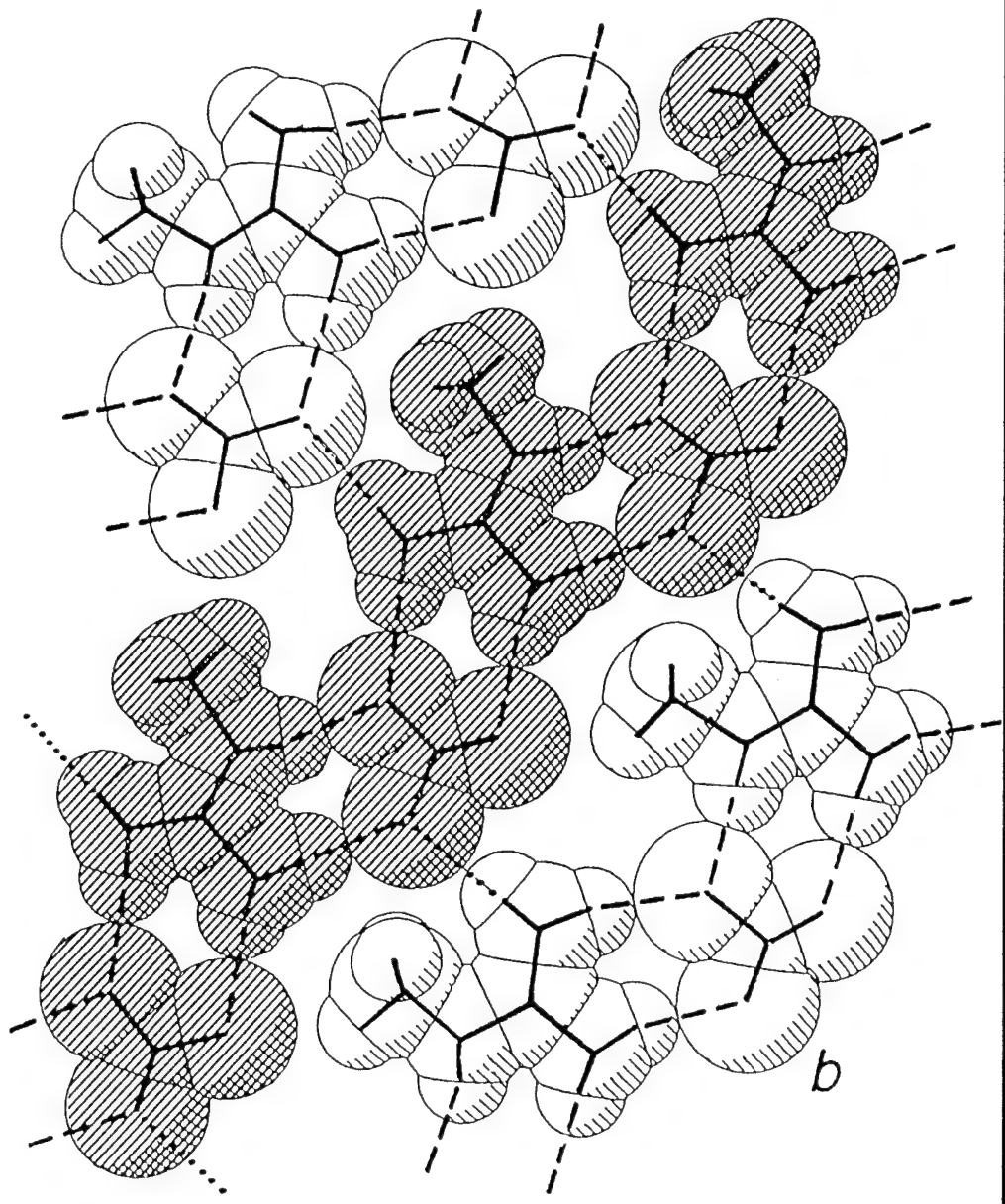

FIG. 4

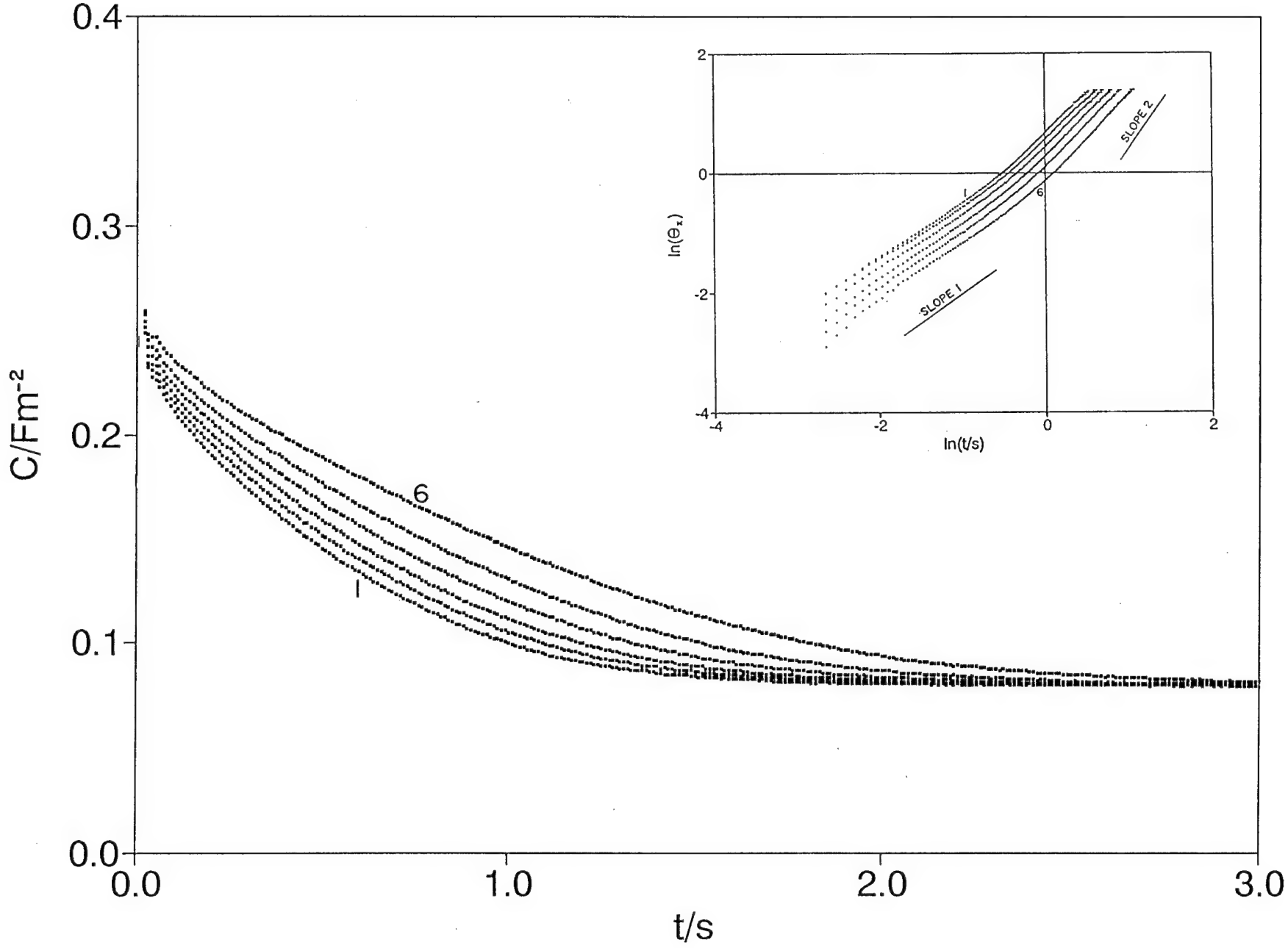
0.4
0.3
0.2
0.1
0.0
C/Fm-2
0.0
1.0
2.0
3.0
t/s
6
1
2
0
-2
-4
ln(Θx)
ln(t/s)
SLOPE 2
SLOPE 1

FIG. 5

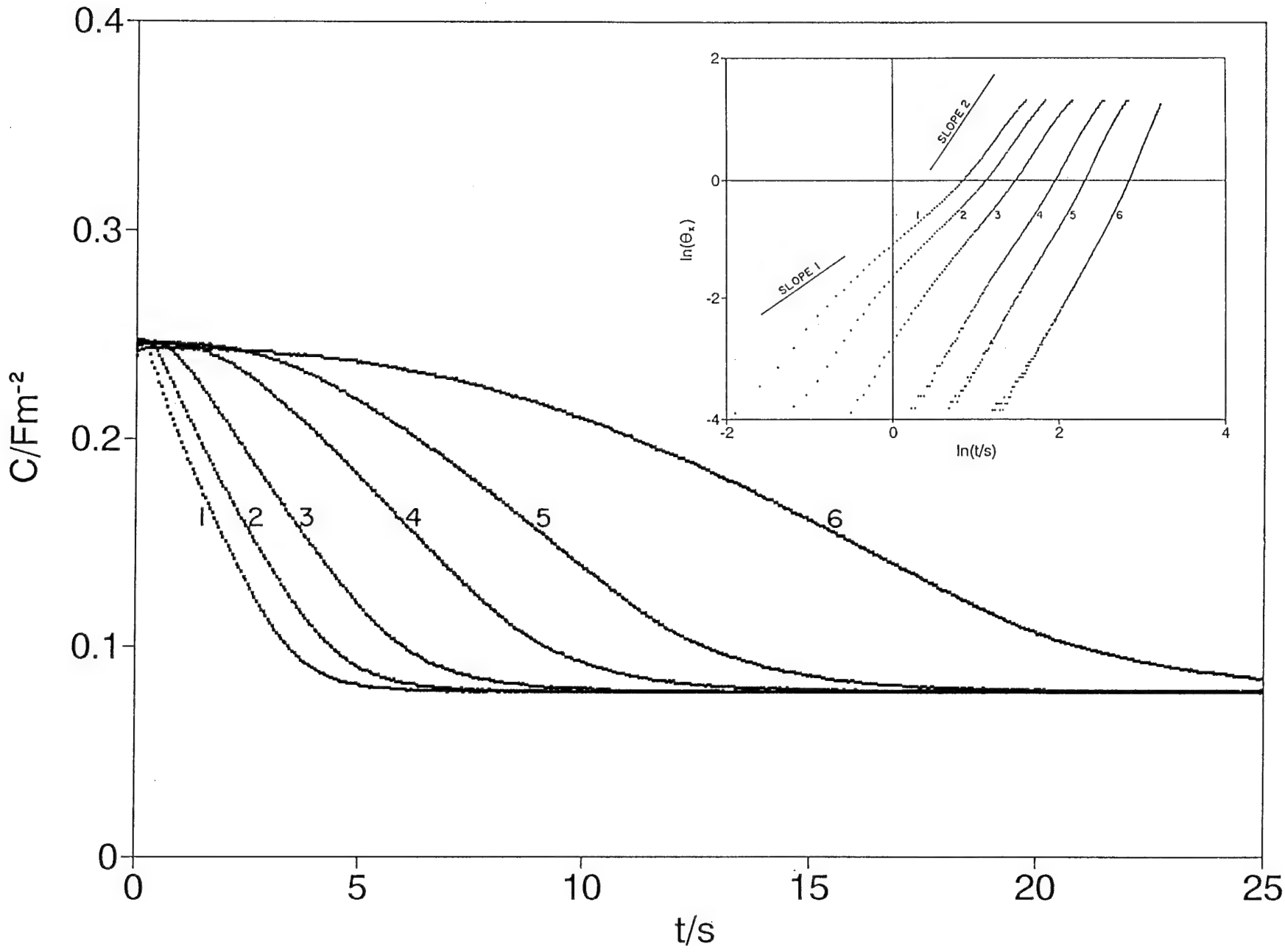
0.4
0.3
0.2
0.1
0
C/Fm-2
0
5
10
15
20
25
t/s
1
2
3
4
5
6
2
0
-2
-4
ln(Θx)
-2
0
2
4
ln(t/s)
SLOPE 2
SLOPE 1

FIG. 6

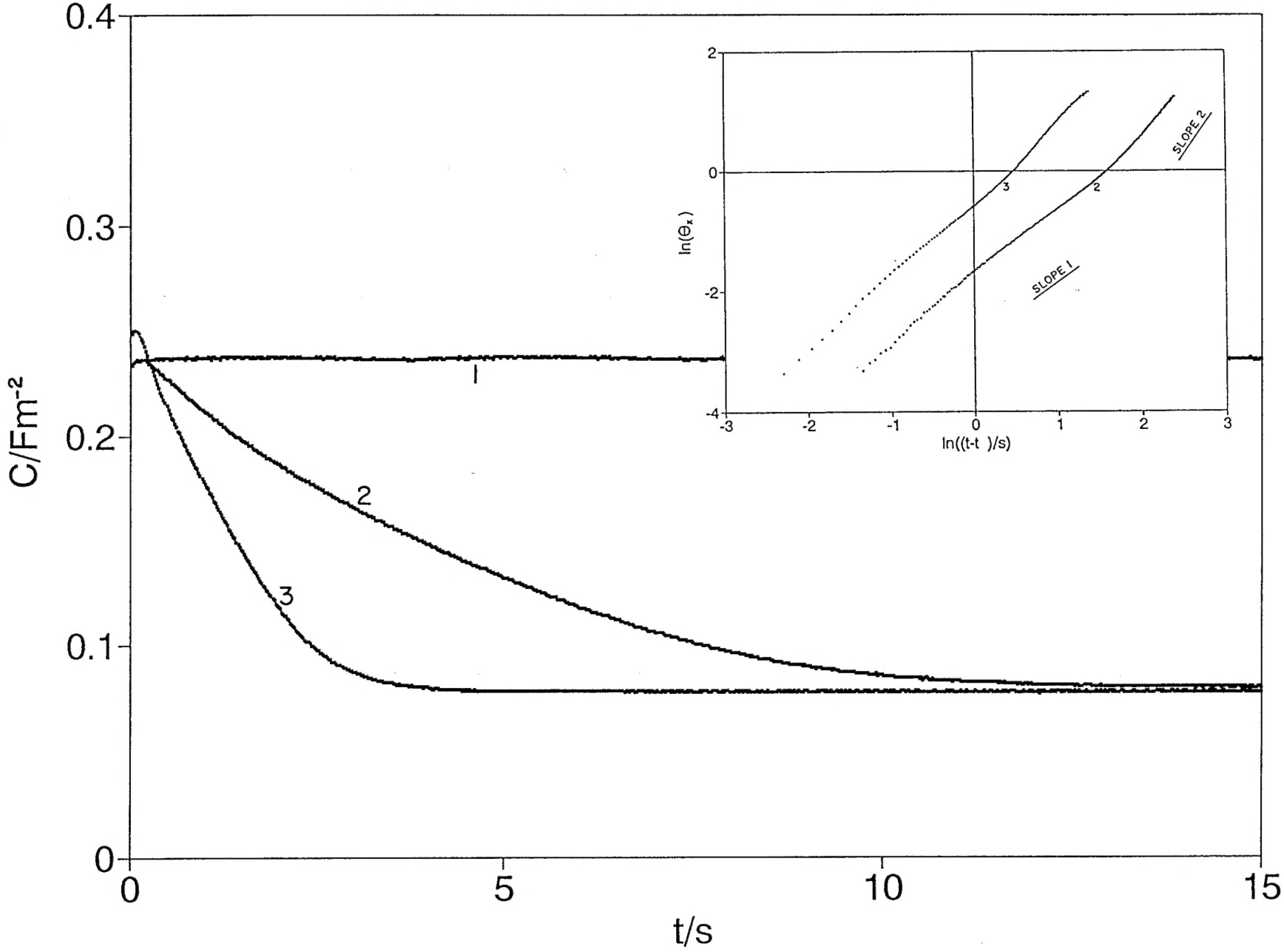
0.4
0.3
0.2
0.1
0
C/Fm-2
0
5
10
15
t/s
1
2
3
2
0
-2
-4
-3
-2
-1
0
1
2
3
ln(Θx)
ln((t-t)/s)
SLOPE 2
SLOPE 1
3
2

FIG. 7

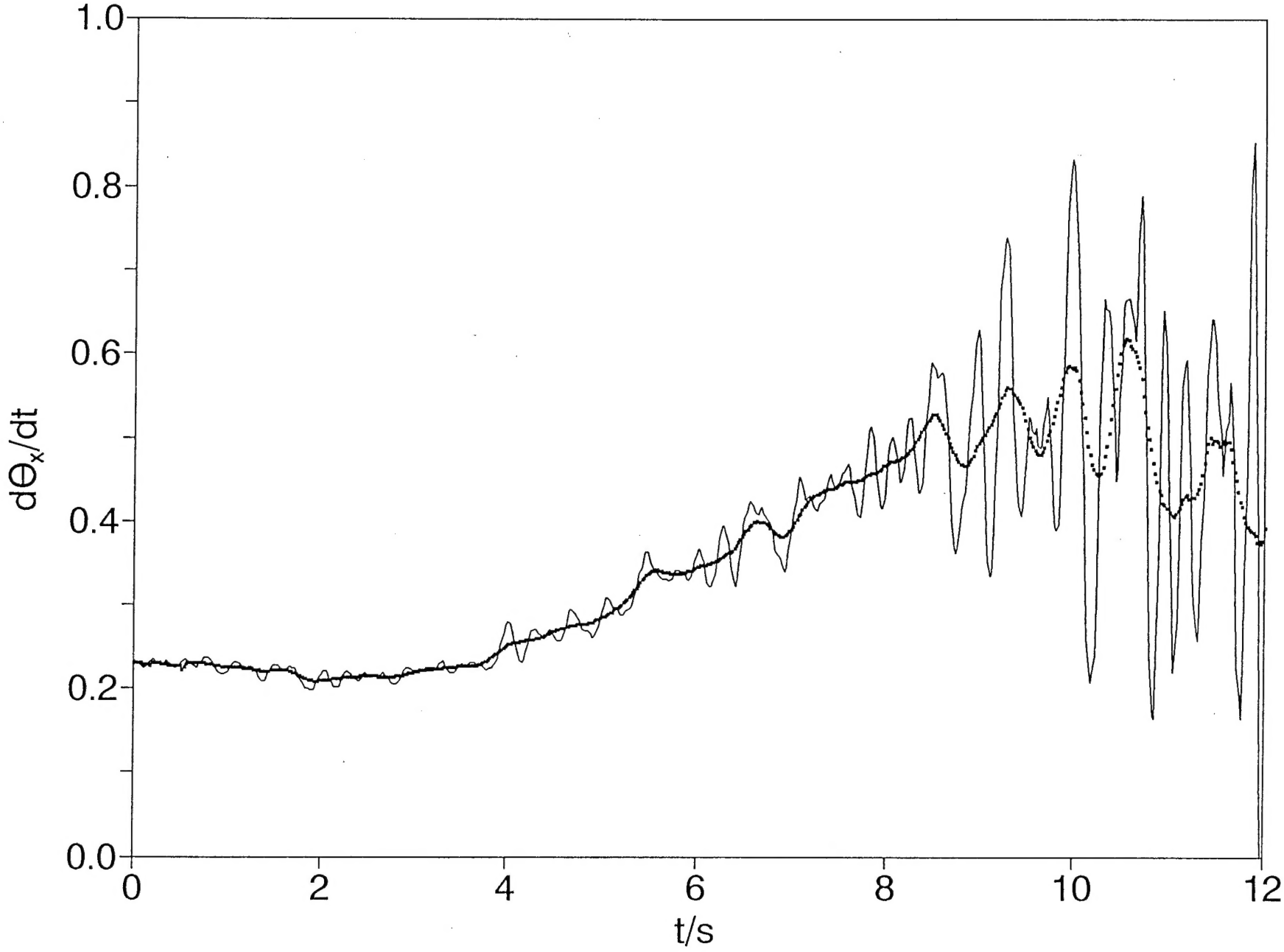

FIG. 8

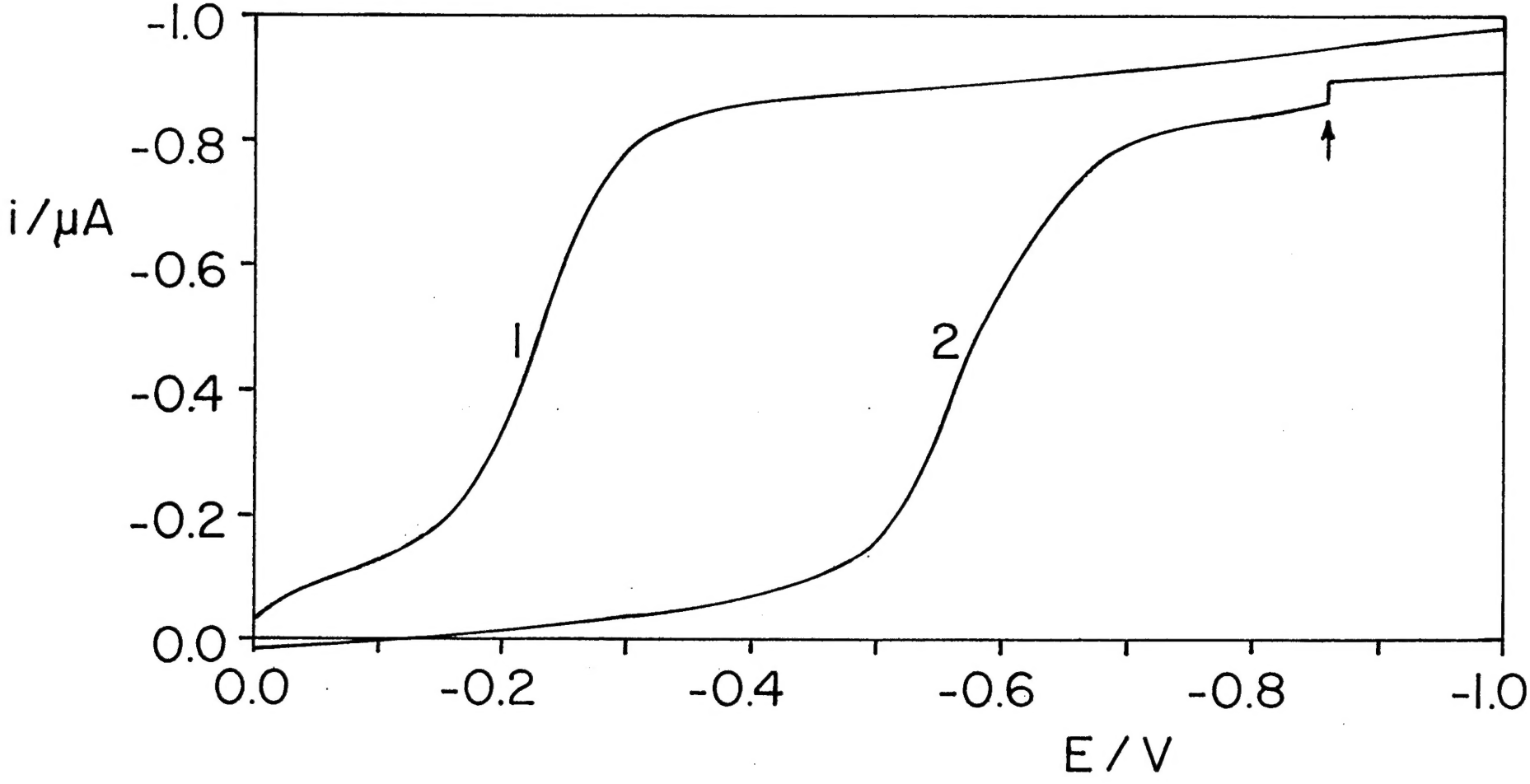

FIG. 9

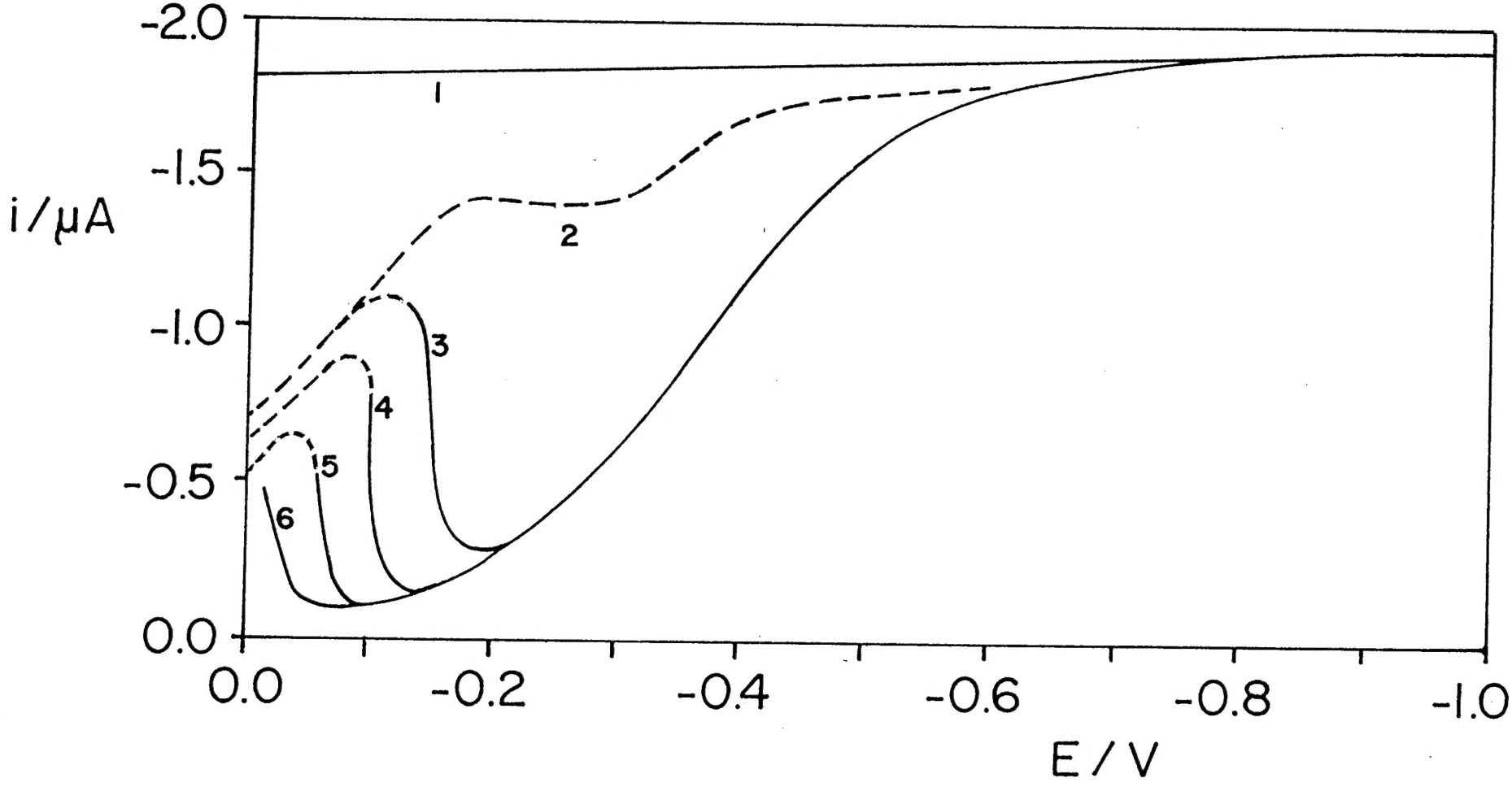

FIG. 10